Chapter 4

Orbital Symmetry of Cobalt Oxides

4.1 Introduction of Na_xCoO_2

Sodium cobalt oxides (Na_xCoO_2) have attracted renewed interest because of their exceptionally large thermoelectric power [1] and the discovery of superconductivity in their hydrated counterparts [2]. Despite intensive experimental [1-9] and theoretical [10-21] works, there remain many unresolved issues concerning the electronic structure of Na_xCoO_2.

Crystal Structure of Na_xCoO_2

Figure 4.1 shows the crystal structure of the Na_xCoO_2[2, 23]. The structure is in hexagonal space group $P6_3/mmc$, as shown in Fig 4.1(A). This compound consists of two-dimensional CoO_2 layers which are separating by a thick layer of Na^+ ions. In each CoO_2 layers, the Co ions are at the center of the octahedra forming a triangular (hexagonal) lattice. Left panel of Fig 4.1(B) shows the undistorted CoO_6 octahedron structure in O_h symme-

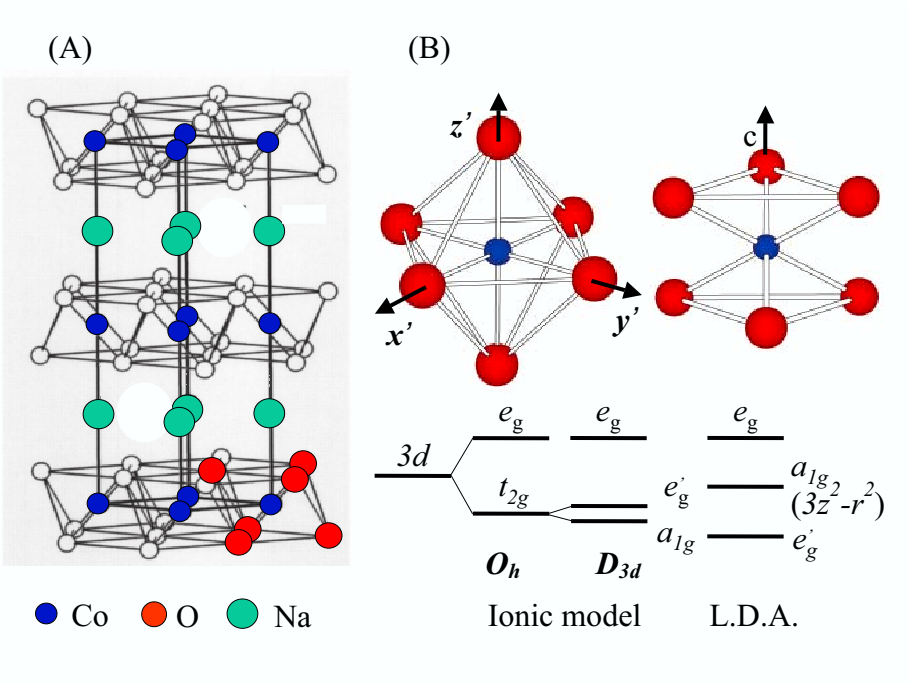

Figure 4.1: (A) Crystal structure of Na_xCoO_2 is hegagonal space group $P6_3/mmc$. The Co atoms are surrounded by six oxygen atoms and form in an octahedral structure. (B) Illustration of the trigonal distortion of a CoO_6 octahedron. Left panel: undistorted CoO_6 octahedron with cubic (O_h) symmetry. Right panel: compressed CoO_6 octahedron with D_{3d} symmetry. The distorted CoO_6 is rotated such that the three-fold rotation axis is along the c-axis. Crystal-field splitting of Co $3d$ states in distorted CoO_6 according to an ionic model and relative energy positions of $3d$ bands obtained from LDA calculations.

try. The oxygen octahedral in Na_xCoO_2 have a trigonal distortion with a compression along the body diagonal direction of the embedding cube. The symmetry of the trigonal distortion of the CoO_6 octahedron is D_{3d}. For convenience, we choose the corresponding body diagonal direction as the c axis, as shown in the right panel of Fig 4.1(B).

Physical Properties of Na_xCoO_2

Terasaki *et al* [1] discovered the enhanced thermopower in the layered Na-doped cobaltate Na_xCoO_2. In addition, Wang *et al* [4] reported the

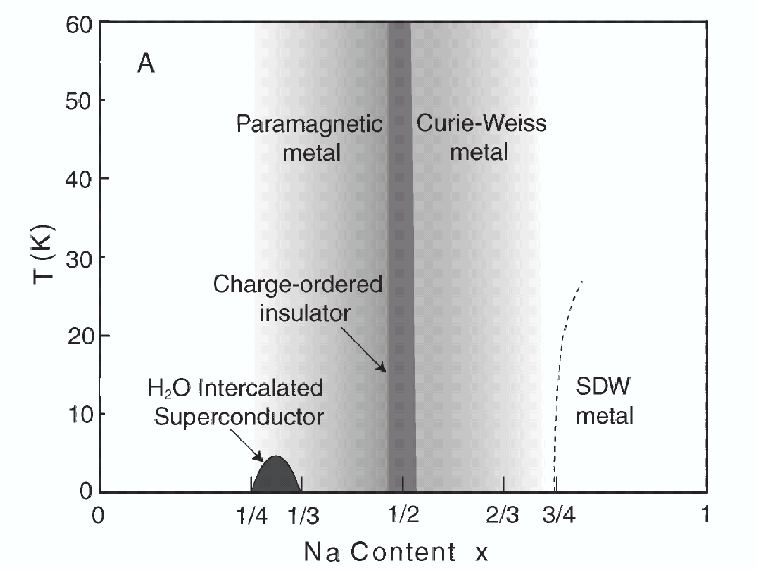

Figure 4.2: The phase diagram of Na_xCoO_2. The charge-order insulator for x=1/2 is between the paramagnetic metal at x=0.3 and the Curie-Weiss metal at x=0.65∼0.75. (from Ref. [7])

thermopower suppression of Na_xCoO_2 (x=0.68) in a 10-Tesla longitudinal magnetic field, and constituted the direct evidence of the large thermopower dominated by spin-entropy terms. Such the enhanced thermopower by spin-entropy in Na_xCoO_2 implies that a strong electron-electron correlation effects is necessary to describe the transport properties.

4.2 Fundamental Issues about Na_xCoO_2

An important issue is the orbital character of the valence electrons responsible for low-energy excitations. The lattice of Na_xCoO_2 exhibits a trigonal distortion, leading to a splitting of t_{2g} states into e'_g and a_{1g} states, as shown in Fig. 4.1(B). Left panel shows the undistorted CoO_6 octahedron structure in O_h symmetry. Right panel displays the trigonal distortion of the

CoO_6 octahedron with D_{3d} symmetry. After the rotation, the new c-axis is the three-fold rotation axis. However, the electronic structure in the trigonal distortion with D_{3d} symmetry, the e'_g states spread over the ab plane, whereas the a_{1g} state extends to the c-axis [22]. Band-structure calculations in the local-density approximation (LDA) show that the a_{1g} state has a one-particle energy higher than that of e'_g and is most relevant to low-energy excitations [10]. These calculations are however different from a crystal-field approach in which the compressed trigonal distortion stabilizes the a_{1g} state [16], as illustrated in Fig. 4.1(B).

Several theoretical works have proposed one-band models to discuss the electronic structure of Na_xCoO_2 [12, 14, 13, 15], rather than multi-band models [16, 17]. The validity of one-band models is a fundamental question for the triangular cobaltates. If the twofold e'_g level is higher than the a_{1g} level, the orbital degree of freedom is indispensable ingredient to understand the electronic states of the material. On the other hand, the states near the Fermi level can be mapped onto a single-band model on the triangular lattice when the a_{1g} level is higher.

To comprehend the effect of electron correlations is also imperative for an understanding of the electronic structure of Na_xCoO_2. Many microscopic models with strong electron correlations explicitly included have been proposed to explain the spectacular properties of Na_xCoO_2 [14, 13, 16, 12, 15, 17]. On the other hand, a recent LDA+U study (LDA including on-site Coulomb energy U) [21] explains the Fermi surface measured by angle-

resolved photoemission [8, 9] and concludes that Na_xCoO_2 is a moderately correlated system. One therefore requires further spectral evidence for strong electron correlations to justify microscopic models of correlated electrons for Na_xCoO_2.

Another subject is whether the electronic states of Na_xCoO_2 responsible for low-energy excitations have O $2p$ character. Early LDA calculations [10] indicate that hybridization between Co $3d$ and O $2p$ in $Na_{0.5}CoO_2$ is weak. Analysis of core-level photoemission results suggests that Na_xCoO_2 has a Mott-Hubbard-like rather than a charge-transfer electronic structure [6]. On the other hand, LDA results corroborated with a Hubbard-like model conclude that $Na_{1/3}CoO_2$ exhibits significant hybridization between Co $3d$ and O $2p$ [18].

Here, we present measurements of soft x-ray absorption spectroscopy (XAS) on Na_xCoO_2 pertinent to its orbital character of the electronic states determining the low-energy physics. To investigate the detailed electronic structure, we discuss the spectral character of strongly correlated electrons of Na_xCoO_2. We also compare Co $2p$ XAS with calculations using a cluster model in the configuration-interaction (CI) approach.

4.3 Polarization-Dependent XAS

Single crystals of $Na_{0.75}CoO_2$ were grown by the travelling solvent floating-zone method. Crystals with smaller Na concentrations of $x = 0.67$ and 0.5 were prepared from $Na_{0.75}CoO_2$ through subsequent electrochemical de-

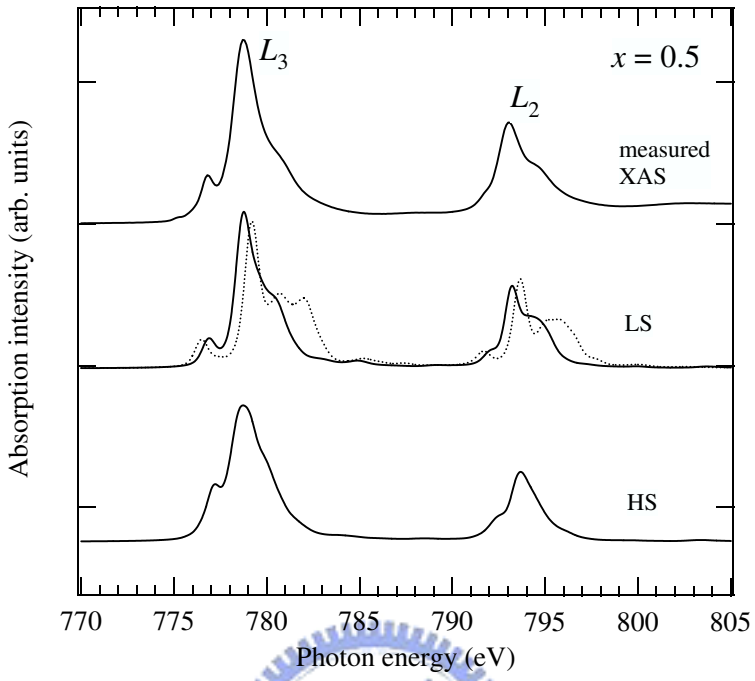

Figure 4.3: Measured and calculated isotropic Co L-edge XAS of $Na_{0.5}CoO_2$. Theoretical Co L-edge XAS spectra for LS and HS Co $3d$ states were broadened with a Gaussian full width of 0.5 eV at half maximum (FWHM) and with a Lorentian FWHM of 0.4 eV. The dotted line is a simulated XAS with the parameters reported in Ref. [6].

intercalation procedures. Details of crystal growth are discussed elsewhere [24]. Crystals were freshly cleaved in vacuum with a pressure lower than 5×10^{-10} torr at 80 K.

4.3.1 Co L-edge XAS

We measured the Co $L_{2,3}$-edge XAS of Na_xCoO_2 to study its detailed electronic structure. Based on a cluster model in the CI approach, we simulated XAS spectra with a superposition of calculated XAS for Co^{4+} and Co^{3+} with weights of $1 - x : x$. To summarize, the shoulder peak on the low-energy side of the L_3 edge arises from the a_{1g} orbital character in the

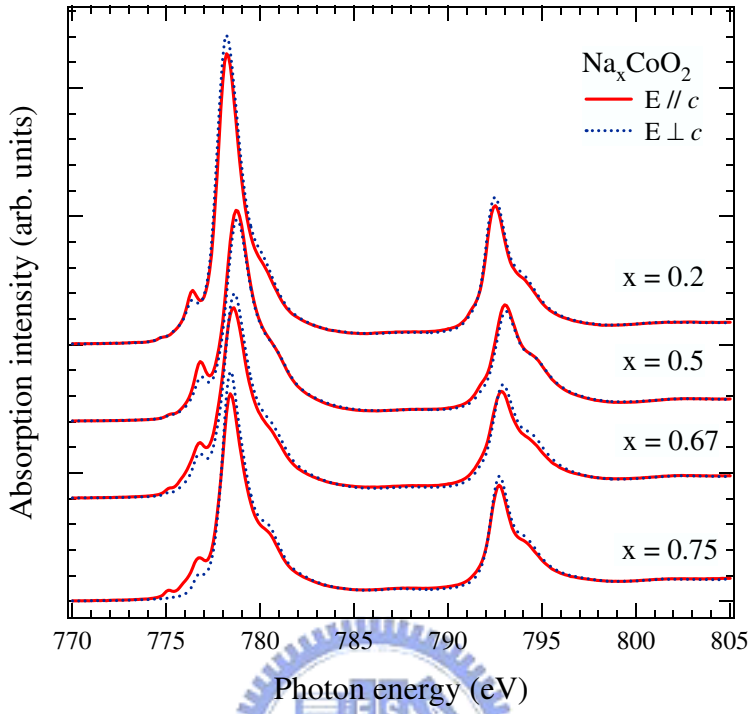

Figure 4.4: Co $L_{2,3}$-edge XAS of various doping $Na_{0.5}CoO_2$. The shoulder peaks on the L_3-edge show strong out-off-plane component.

ground state. Comparing the Co L-edge XAS of x =0.5, 0.67, and 0.75 with CI calculations using a series of parameters, we found that the calculated XAS for Co ions in a low-spin (LS) state resembles the measured XAS satisfactorily, but the calculated XAS for high-spin (HS) ions is inconsistent with the measurement, as demonstrated in Fig. 4.3 for $x = 0.5$ [33]. The calculations indicate that Na_xCoO_2 has a charge-transfer energy smaller than the on-site Coulomb energy (U_{dd}=4.5 eV). In particular, because of the high valency, Co^{4+} ions have a negative charge-transfer energy ($\Delta \sim -1$ eV) [34], in contrast to the conclusion from the analysis of core-level photoemission data [6]. Calculations with the parameters that Chainani *et al.* concluded

(U_{dd}=5.5, Δ=4.0, $10Dq = 2.5$ for Co^{3+}, and $10Dq = 4.0$ for Co^{4+} in units of eV [6]) give rise to a Co $2p$ XAS inconsistent with our measurements, as in Fig. 4.3.

Further, Fig. 4.4 display the polarization-dependent Co L-edge XAS of Na_xCoO_2 with various Na doping. The spectra are normalized at 850 eV at wich Co $2p$ XAS has no doping-dependent structure. The Co $2p$ XAS spectra show that the shoulder peaks at photon energy 777 eV have a strong z component. In shortly, this shoulder peak on the L_3-edge arises from the a_{1g} band with $3z^2 - r^2$ orbital character in the ground state. Comparing with the Fig 4.1 (B), the band-structure calculation in LDA is consistent with our polarization-dependent Co L-edge XAS results, where the low-energy excitation exhibits a_{1g} symmetry.

4.3.2 O K-edge XAS

Figure 4.5 presents isotropic O $1s$ XAS of $Na_{0.5}CoO_2$ single crystals; our spectrum is similar to those of polycrystalline samples [25]. O $1s$ XAS measures transitions from an O $1s$ core level to unoccupied O $2p$ states mixing with bands of primary Co or Na character. The structure in XAS near the threshold arises from covalent mixing of Co $3d$ and O $2p$. One can interpret such a near-edge structure as a one-electron addition process, i.e., $d^n \rightarrow d^{n+1}$, if the influence of the O $1s$ core hole is neglected [26, 27]. We observed three pronounced O $1s$ XAS peaks in the vicinity of the threshold, implying strong hybridization between O $2p$ and Co $3d$ and many O $2p$ holes existing in

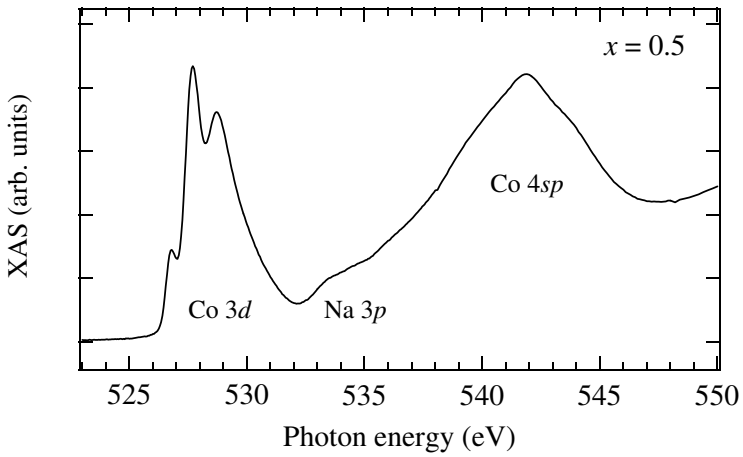

Figure 4.5: O 1s XAS spectrum of $Na_{0.5}CoO_2$ measured in the total electron yield mode. The unoccupied bands with which O 2p states hybridize are denoted in the plot.

$Na_{0.5}CoO_2$. The broad feature about 540 eV corresponds to Co 4sp bands; the features in the region about 535 eV are attributed to transitions involving Na 3p.

Further, we performed the polarization-dependent O K-edge XAS of Na_xCoO_2 with various Na dopings, as shown in Fig. 4.6. The detail of three pronounced peaks at photon energy from 526 eV to 532 eV, which indicated the hybridization between O 2p and Co 3d, will be described after. At the photon energy about 535 eV, the excitations into unoccupied O 2p levels reveal the hybridization between O 2p and Na 3p. As shown in Fig 4.6, the resulting peaks near 534 eV are strong polarization-dependent and the absorption intensities of $\mathbf{E} \parallel c$ are stronger than that of $\mathbf{E} \perp c$. This result indicates that the hybridization between Na and O is along z direction and result in three dimensional hybrid magnetism. From our XAS results, the inter-plane binding is more likely to have a covalent binding rather than ionic

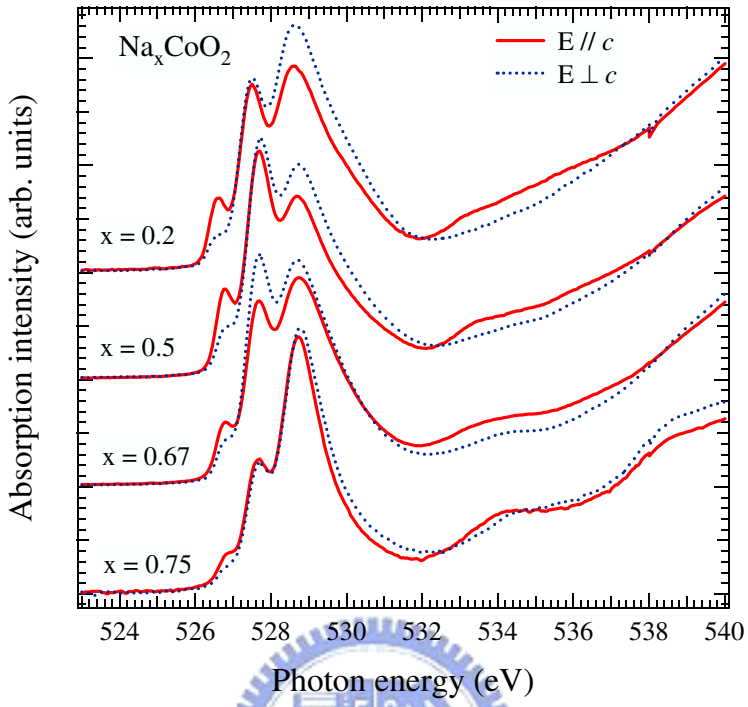

Figure 4.6: Doping and polarization-dependent O K-edge XAS of Na_xCoO_2. The broad features about 534 eV show the hybridization between Na and O.

character.

As for determining the symmetry of electronic states governing the low-energy excitations, we resorted to measurements of polarization-dependent O 1s XAS of $Na_{0.5}CoO_2$, as plotted in Fig. 4.7. The O 1s XAS shows that the lowest-energy peak at 526.8 eV (labelled as A) has a strong z component. The ratio $I_\perp/I_\parallel$ for peak A is 0.37 ± 0.05, as depicted in the inset of Fig. 3. The in-plane components of two other peaks at 527.6 eV and 528.7 eV (labelled as A′ and B, respectively) are slightly larger than their corresponding z components.

The polarization dependencies of peaks A, A′ and B in the O 1s XAS

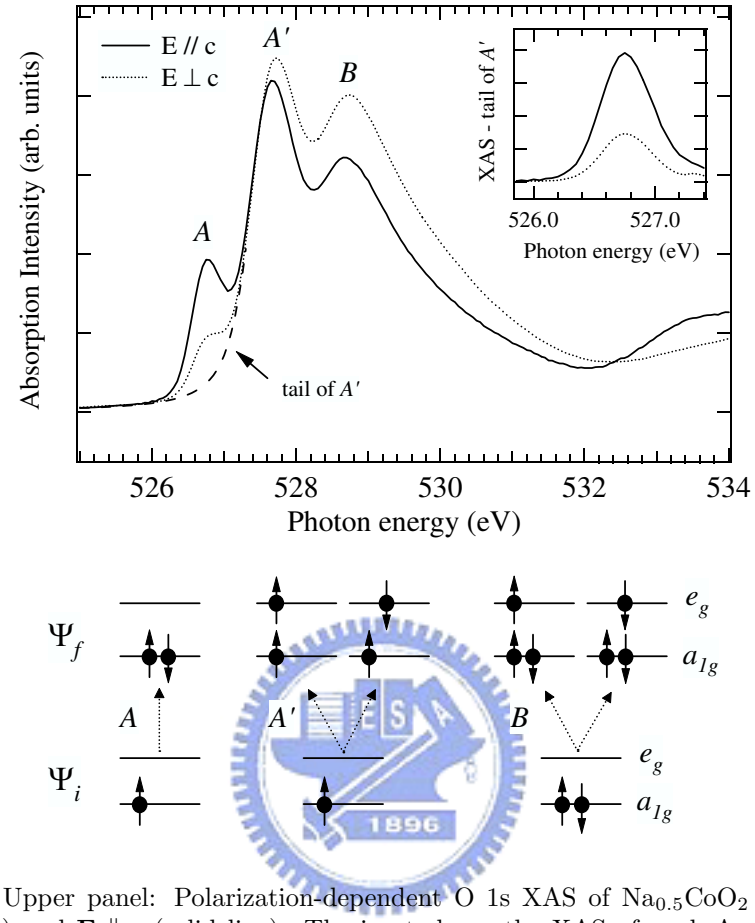

Figure 4.7: Upper panel: Polarization-dependent O 1s XAS of $Na_{0.5}CoO_2$ with $\mathbf{E} \perp c$ (dotted line) and $\mathbf{E} \parallel c$ (solid line). The inset shows the XAS of peak A after removal of background from the tail of peak A′ (dashed line). Lower panel: Energy diagrams illustrating transitions from Ψ_i in the low-spin state to Ψ_f corresponding to the symmetries of peaks A, A′ and B. The e_g' states are omitted for clarity.

depend on hybridization between Co 3d and O 2p. Qualitatively, the hybridization results from the inter-atomic matrix element V_{pd} between Co 3d and O 2p, which can be expressed in terms of the Slater-Koster transfer integrals $pd\sigma$ and $pd\pi$ [28]; the ratio $I_\perp/I_\parallel$ is proportional to the ratio of the averaged V_{pd}^2 with O 2p orbitals perpendicular and parallel to the c-axis. For an undistorted lattice, $I_\perp/I_\parallel$ of O 1s XAS with a final state of a_{1g} symmetry is 0.25, while that of e_g symmetry is 1.0, if one uses an empirical

relation $pd\sigma = -(4/\sqrt{3})pd\pi$. $I_\perp/I_\parallel$ depends also on the distortion and the band effect. If the compressed trigonal distortion of a Na_xCoO_2 lattice is taken into account, O 1s XAS with final states of a_{1g} symmetry has a large out-of-plane polarization, whereas that with e_g symmetry has an in-plane polarization. Thus, our measurements that peak A and A$'$ have opposite polarizations show that peak A results predominantly from adding an electron to a state of a_{1g} symmetry, whereas peaks A$'$ and B correspond to adding electrons to states of e_g symmetry, as illustrated in the lower panel of Fig. 4.7. In other words, the symmetries of the transitions associated with peaks A, A$'$ and B correspond mainly to $(a_{1g})^1 \rightarrow (a_{1g})^2$, $(a_{1g})^1 \rightarrow (a_{1g})^1(e_g)^1$, and $(a_{1g})^2 \rightarrow (a_{1g})^2(e_g)^1$, respectively. Note that we omit the low-spin $(e_g')^4$ in the above expressions for clarity. These observations reveal that the electronic states of predominantly a_{1g} symmetry determine the low-energy excitations of Na_xCoO_2. Moreover, our observation of the a_{1g} symmetry of the states crossing the Fermi level suggests a significant hybridization between O 2p and Co 3d, because hopping of a_{1g} states within the CoO_2 layer would be difficult without O 2p mixing. Hence, one expects that the ground-state configurations for Co^{4+} and Co^{3+} in Na_xCoO_2 have significant weights of $d^6\underline{L}$ and $d^7\underline{L}$, respectively, in which $\underline{L}$ denotes an oxygen 2p hole.

To seek spectral evidence for electron correlations of 3d bands, we plot doping-dependent isotropic O 1s XAS of Na_xCoO_2 in Fig. 4.8. The spectra are normalized to have the same intensity at 600 eV at which O 1s XAS has no doping-dependent structure. We found a spectral-weight transfer in the

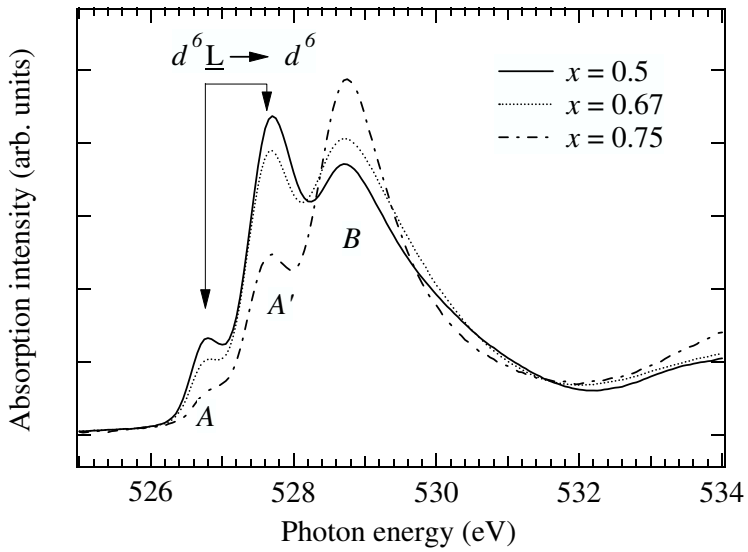

Figure 4.8: Doping-dependent isotropic O 1s XAS of Na_xCoO_2, i.e., $(I_\parallel + I_\perp)/2$. The dominant transitions $d^6\underline{L} \rightarrow d^6$ leading to the peaks A and A′ are indicated in the figure.

doping-dependent O 1s XAS; as the doping x increases, the intensities of peaks A and A′ decrease, but peak B increases in intensity. Such a spectral-weight transfer is in contrast to the picture of rigid-band shift in which the spectral weight associated with a_{1g} bands is influenced only by the position of the Fermi level. The decrease (increase) in the intensity of peaks A and A′ (peak B) with the increase of doping indicates that the XAS peaks are derived from Co^{4+} (Co^{3+}), because a fraction x of Co^{4+} changes to Co^{3+} when the hypothetical CoO_2 is doped with Na. Our results thus suggest that the peaks A and A′ (peak B) originate from O 2p hybridized with 3d states of Co^{4+} (Co^{3+}) and correspond to adding electrons to the states of a_{1g} and e_g symmetries associated with Co^{4+} (e_g symmetry associated with Co^{3+}), further supporting the symmetry assignment from the polarization-dependent mea-

surements discussed above. The spectral-weight transfer of the one-electron addition observed in Na_xCoO_2 is a general feature of strongly correlated systems [29], as in electron-energy loss experiments [30] and O 1s XAS [31] study of $La_{2-x}Sr_xCuO_4$. Such behavior has been found in Li-doped NiO as well [32]. Both $La_{2-x}Sr_xCuO_4$ and $Li_xNi_{1-x}O$ are charge-transfer systems; thus Na_xCoO_2 is expected to have a charge-transfer electronic structure.

Spectral-weight transfer observed in O 1s XAS also manifests the doping-dependent p-d hybridization in Na_xCoO_2. The p-d hybridization determines the e_g occupation in the ground state and the change in the O 1s XAS intensities of different Na concentrations. As the Na doping changes from $x = 0.5$ to $x = 0.75$, the increase in the intensity of peak B is smaller than the decrease of peak A′, demonstrating the reduction of p-d hybridization and e_g occupation with the increase of doping. Our results agree with recent LDA calculations [18] which conclude that, as the doping increases, the increase of t_{2g} electrons are dressed by e_g holes. Thus Na_xCoO_2 exhibits a charge-transfer electronic character rather than a Mott-Hubbard character; the $d^6\underline{L}$ configuration dominates the ground state of Co^{4+} in Na_xCoO_2 [35], like Co^{4+} in $SrCoO_3$ [36] and $La_{1-x}Sr_xCoO_3$ [37]. These results suggest that peaks A and A′ of Fig. 4.8 are derived from transitions of $d^6\underline{L} \rightarrow d^6$ and that the empty a_{1g} band to which the doped electrons go has predominantly O 2p character.

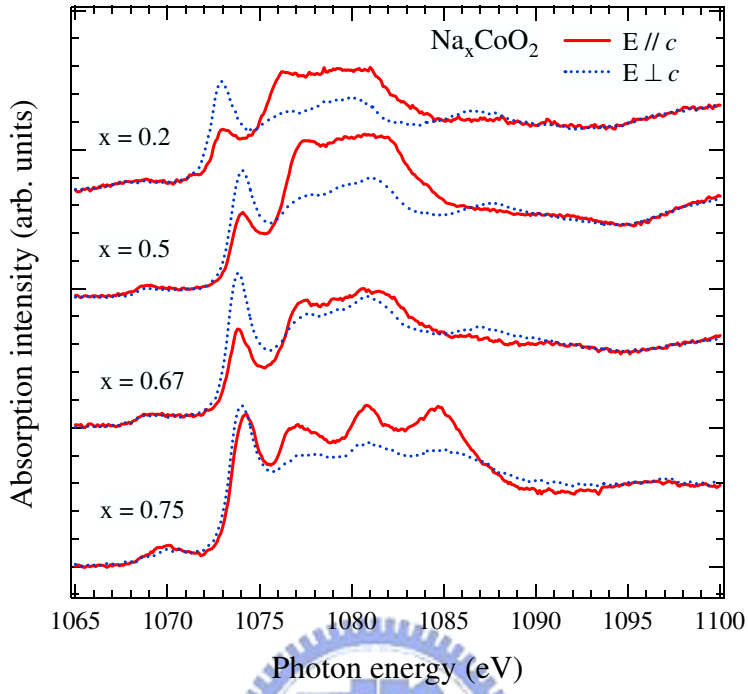

Figure 4.9: Doping and polarization-dependent Na K-edge XAS of Na_xCoO_2. At 1074 eV absorption peaks, the intensity for $\mathbf{E} \perp c$ is stronger than for $\mathbf{E} \parallel c$.

4.3.3 Na K-edge XAS

In order to confirm the broad features in the region about 535 eV in Fig. 4.6, which are attributed to transitions involving Na $3p$, we performed the polarization-dependent Na K-edge XAS of Na_xCoO_2 with various doping, as shown in Fig 4.9. The intensity with $\mathbf{E} \parallel c$ is stronger than that with $\mathbf{E} \perp c$, indicating that the broad feature about 1075∼1085 eV shows a strong out-off-plane character. As comparing with Fig. 4.6, these results also indicate that the Na hybridizes with O along the z direction. Furthermore, the absorption peak at the photon energy of 1073 eV shows a strong in-plane character which corresponds to the spectra at 531 eV in Fig. 4.6. Our XAS results indicate

that the hybridization between Na $3p$ and O $2p$, mediating the inter-layer coupling between CoO_2 planes. In addition, the increase in the width of $3p$ band about 1075∼1085 eV with increasing of the Na doping indicates that the $3p$ electronic states of Na are more delocalized in the high doping case than those in the low Na concentration.

4.4 Conclusions

In conclusion, measurements of doping-dependent O $1s$ XAS provide a spectral fingerprint for strong electron correlations of Na_xCoO_2. Our results reveal the charge-transfer electronic character of Na_xCoO_2; the doping of Na strongly affects the O $2p$ hole density. The electronic states responsible for the low-energy excitations of Na_xCoO_2 have predominantly a_{1g} symmetry with significant O $2p$ character for $x \geq 0.5$.

Reference

[1] I. Terasaki, Y. Sasago, and K. Uchinokura, Phys. Rev. B **56**, R12685 (1997).

[2] K. Takada, H. Sakurai, E. Takayama-Muromachi, F. Izumi, R. A. Dilanian, and T. Sasaki, Nature **422**, 53 (2003).

[3] R. Ray, A. Ghoshray, K. Ghoshray, and S. Nakamura , Phys. Rev. B **59**, 9454 (1999).

[4] Y. Wang, N. S. Rogado, R. J. Cava, and N. P. Ong , Nature **423**, 425 (2003).

[5] T. Motohashi, R. Ueda, E. Naujalis, T. Tojo, I. Terasaki, T. Atake, M. Karppinen, and H. Yamauchi, Phys. Rev. B **67**, 064406 (2003).

[6] A. Chainani,T. Yokoya, Y. Takata, K. Tamasaku, M. Taguchi, T. Shimojima, N. Kamakura, K. Horiba, S. Tsuda, S. Shin, D. Miwa, Y. Nishino, T. Ishikawa, M. Yabashi, K. Kobayashi, H. Namatame, M. Taniguchi, K. Takada, T. Sasaki, H. Sakurai, and E. Takayama-Muromachi, Phys. Rev. B **69**, 180508(R) (2004).

[7] M. L. Foo, Yayu Wang, Satoshi Watauchi, H. W. Zandbergen, Tao He, R. J. Cava, and N. P. Ong, Phys. Rev. Lett. **92**, 247001 (2004).

[8] M. Z. Hasan, Y.-D. Chuang, D. Qian, Y. W. Li, Y. Kong, A. Kuprin, A. V. Fedorov, R. Kimmerling, E. Rotenberg, K. Rossnagel, Z. Hussain, H. Koh, N. S. Rogado, M. L. Foo, and R. J. Cava, Phys. Rev. Lett. **92**, 246402 (2004).

[9] H.-B. Yang, S.-C. Wang, A. K. P. Sekharan, H. Matsui, S. Souma, T. Sato, T. Takahashi, T. Takeuchi, J. C. Campuzano, R. Jin, B. C. Sales, D. Mandrus, Z. Wang, and H. Ding, Phys. Rev. Lett. **92**, 246403 (2004).

[10] D. J. Singh, Phys. Rev. B **61**, 13397 (2000).

[11] D. J. Singh, Phys. Rev. B **68**, 020503(R) (2003).

[12] Y. Tanaka, Y. Yanase, and M. Ogata, cond-mat/0311266.

[13] G. Baskaran, Phys. Rev. Lett. **91**, 097003 (2003).

[14] Q.-H. Wang, D.-H. Lee, and P. A. Lee, Phys. Rev. B **69**, 092504 (2004).

[15] B. Kumar and B. S. Shastry, Phys. Rev. B **68**, 104508 (2003); O. I. Motrunich and Patrick A. Lee, *ibid* **69**, 214516 (2004).

[16] W. Koshibae and S. Maekawa, Phys. Rev. Lett. **91**, 257003 (2003).

[17] Y. Yanase, M. Mochizuki, and M. Ogata, cond-mat/0407563.

[18] C. A. Marianetti, G. Kotliar, and G. Ceder, Phys. Rev. Lett. **92**, 196405 (2004).

[19] L. J. Zou, J.-L. Wang, and Z. Zeng, Phys. Rev. B **69**, 132505 (2004).

[20] P. Zhang, W. Luo, V. H. Crespi, M. L. Cohen, and S. G. Louie, Phys. Rev. B **70**, 085108 (2004).

[21] P. Zhang, W. Luo, M. L. Cohen, and S. G. Louie, Phys. Rev. Lett. **93**, 236402 (2004).

[22] If the z-axis is along the c-axis, a_{1g} is $d_{3z^2-r^2}$; e'_g are $\frac{1}{\sqrt{3}}(d_{yz}+\sqrt{2}d_{xy})$ and $\frac{1}{\sqrt{3}}(d_{zx}-\sqrt{2}d_{x^2-y^2})$.

[23] J. D. Jorgensen, M. Avdeev, D. G. Hinks, J. C. Burley, and S. Short, Phys. Rev. B **68**, 214517 (2003).

[24] F. C. Chou, J. H. Cho, P. A. Lee, E. T. Abel, K. Matan, and Y. S. Lee, Phys. Rev. Lett. **92**, 157004 (2004).

[25] W.-S. Yoon, K. -B. Kim, M. -G. Kim, M. -K. Lee, H. -J. Shin, J. -M. Lee, J. -S. Lee, and C. -H. Yo, J. Phys. Chem. B **106**, 2526-2532 (2002) ; M. Kubota, K. Takada, T. Sasaki, H. Kumigashira, J. Okabayashi, M. Oshima, M. Suzuki, N. Kawamura, M. Takagaki, K. Fukuda, and K. Ono, Phys. Rev. B **70**, 012508 (2004).

[26] F. M. F. de Groot, M. Grioni, J. C. Fuggle, J. Ghijsen, G. A. Sawatzky, and H. Petersen, Phys. Rev. B **40**, 5715 (1989).

[27] J. van Elp and A. Tanaka, Phys. Rev. B **60**, 5331 (1999).

[28] J. C. Slater and G. F. Koster, Phys. Rev. **94**, 1498 (1954).

[29] H. Eskes, M. B. J. Meinders, and G. A. Sawatzky, Phys. Rev. Lett. **67**, 1035 (1991).

[30] H. Romberg, M. Alexander, N. Nucker, P. Adelmann, and J. Fink, Phys. Rev. B **42**, 8768 (1990).

[31] C. T. Chen, F. Sette, Y. Ma, M. S. Hybertsen, E. B. Stechel, W. M. C. Foulkes, M. Schluter, S. -W. Cheong, A. S. Cooper, L. W. Rupp, Jr., B. Batlogg, Y. L. Soo, Z. H. Ming, A. Krol, and Y. H. Kao, Phys. Rev. Lett. **66**, 104 (1991).

[32] P. Kuiper, G. Kruizinga, J. Ghijsen, G. A. Sawatzky, and H. Verweij, Phys. Rev. Lett. **62**, 221 (1989).

[33] Parameters (in units of eV): U_{dd}=4.5, U_{dc}=5.5, Δ=3.5 (for Co^{3+}), $\Delta=-1.0$ (for Co^{4+}), $10Dq$=1.5 (for LS), $10Dq$=0.5 (for HS), V_{eg}=3.5, T_{pp}=0.7, $D_{trg}=-1.0$, and $Q_{mix}=0.5$, where $D_{trg}\equiv E(e'_g)-E(a_{1g})$; Q_{mix} is the hybridization between e'_g and e_g.

[34] Δ for Co^{4+} is defined as $E(3d^6\underline{L})-E(3d^5)$.

[35] The ground-state configurations for LS Co^{4+} are d^5=15.9%, $d^6\underline{L}$=48.1%, $d^7\underline{L}^2$=31.1%, and $d^8\underline{L}^3$=4.9%; those for LS Co^{3+} are d^6=43.2%, $d^7\underline{L}$=46.9%, and $d^8\underline{L}^2$=9.9%.

[36] R. H. Potze, G. A. Sawatzky, and M. Abbate, Phys. Rev. B **51**, 11501 (1995).

[37] T. Saitoh, T. Mizokawa, A. Fujimori, M. Abbate, Y. Takeda, and M. Takano, Phys. Rev. B **56**, 1290 (1997).